COMMUNICATIONS: SIF Congress 2014

(Anti-)deuteron production at the LHC with the ALICE-HMPID detector

F. BARILE for the ALICE COLLABORATION

INFN, Sezione di Bari - Bari, Italy
Dipartimento di Fisica, Università degli Studi di Bari - Bari, Italy

Summary. — The high center-of-mass energies delivered by the LHC during the last three years of operation led to accumulate a significant statistics of light (hyper-)nuclei in pp, p-Pb and Pb-Pb collisions. The ALICE apparatus allows for the detection of these rarely produced particles over a wide momentum range thanks to its excellent vertexing, tracking and particle identification capabilities. The last is based on the specific energy loss in the Time Projection Chamber and the velocity measurement with the Time-Of-Flight detector. The Cherenkov technique, exploited by a small acceptance detector (HMPID), has been also recently used for the most central Pb-Pb collisions to extend the identification range of the (anti-)deuteron at intermediate transverse momentum. An overview of the recent results on the (anti-)deuteron production in pp, p-Pb and Pb-Pb collisions measured with ALICE experiment are presented, giving a particular emphasis to the description of the Cherenkov technique.

PACS `29.40.Ka` – Cherenkov detectors.
PACS `12.38.Mh` – Quark-gluon plasma.
PACS `25.75.-q` – Relativistic heavy-ion collisions.
PACS `12.38.Aw` – General properties of QCD (dynamics, confinement, etc.).

1. – Introduction

Collisions of ultra-relativistic heavy ions provide a unique experimental condition to produce nuclei and hypernuclei thanks to the large amount of energy deposited into a volume much larger than in pp collisions. The measurements presented here, have been performed in Pb-Pb collisions at $\sqrt{s_{\mathrm{NN}}} = 2.76\,\mathrm{TeV}$ as a function of collision centrality and in p-Pb collisions at $\sqrt{s_{\mathrm{NN}}} = 5.02\,\mathrm{TeV}$ as a function of charged-particle multiplicity. The unique particle identification capabilities of the ALICE detector [1] system is suited to measure nuclei and hypernuclei and for the search of exotic states like Λn bound states and the H-dibaryon. The production mechanisms of these particles are typically discussed within two approaches: the statistical thermal model and the coalescence model.
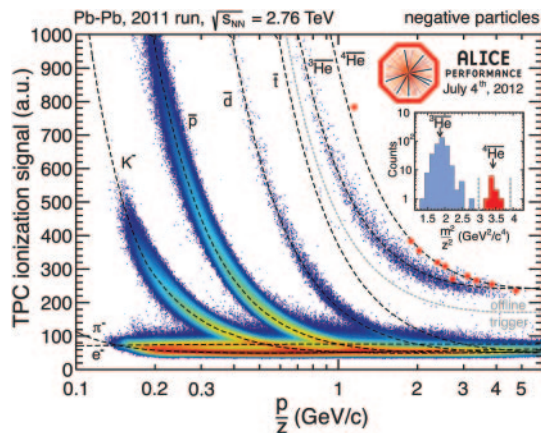
Fig. 1. – Specific energy loss (dE/dx) in the TPC *vs.* rigidity in Pb-Pb collisions at $\sqrt{s_{\mathrm{NN}}} =$ 2.76 TeV. The lines show the parametrization of the expected mean energy loss.

In the thermal model [2-4] the chemical freeze-out temperature T_{chem} acts as the key parameter at LHC energies. The strong sensitivity of the nuclei production to the choice of T_{chem} is caused by the large mass m and the exponential dependence of the yield given by the factor $\exp(-m/T_{\mathrm{chem}})$. In the coalescence model, nuclei are formed by protons and neutrons which are nearby in space and exhibit similar velocities [5,6]. A quantitative description of this process, applied to many collision systems at various energies [7-15], is typically formulated in terms of the coalescence parameter B_{A} (see sect. **3**).

2. – Particle identification in ALICE and the HMPID detector

In this section the particle identification (PID) detectors relevant for the analysis presented in this contribution are briefly described. Particular attention to the HMPID detector will be given. A detailed review of the ALICE experiment and its PID capabilities can be found in [1, 16, 17].

The Inner Tracking System (ITS) is a six-layered silicon detector with radii ranging between 3.9 cm and 43 cm. The precise space-point resolution in the silicon layers allows a precise separation of primary and secondary particles (better than 300 μm) in the high track density region close to the primary interaction vertex. Four out of the six layers measure the particle specific energy loss per unit length (dE/dx) and are used for particle identification in the non-relativistic region.

The Time Projection Chamber (TPC) is the main central-barrel tracking detector of ALICE. It is a large-volume high-granularity cylindrical detector that provides three-dimensional hit information and dE/dx measurement with up to 159 samples. It can measure charged-particle abundances on a statistical basis also in the relativistic rise for momenta up to 50 GeV/c. Figure 1 shows the specific energy loss (dE/dx) in the TPC *vs.* rigidity (p/z) in Pb-Pb collisions at $\sqrt{s_{\mathrm{NN}}} = 2.76$ TeV.

The Time Of Flight (TOF) detector is a large area array devoted to particle identification in the intermediate momentum range using the information on the velocity of the particle to identify them within an acceptance similar to that of the TPC. The total time-of-flight resolution for tracks in Pb-Pb collisions is about 80 ps.
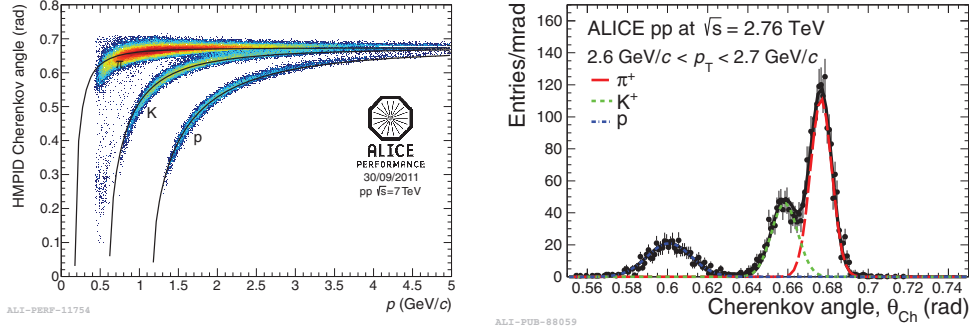
Fig. 2. – Left: Cherenkov angle from HMPID as a function of momentum in pp collisions at $\sqrt{s} = 7\,\mathrm{TeV}$. Right: an example of the Cherenkov angle distribution measured in the HMPID for positive tracks in a narrow p_T interval in pp collisions at $\sqrt{s} = 2.76\,\mathrm{TeV}$.
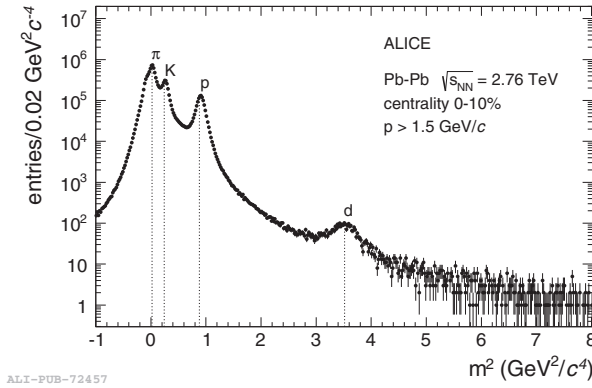

Fig. 3. – Squared particle masses calculated from the momentum and Cherenkov angle reconstructed with ITS-TPC and HMPID, respectively, in central Pb-Pb collisions at $\sqrt{s_{\mathrm{NN}}} = 2.76\,\mathrm{TeV}$. Dotted lines indicate the PDG mass values. The pion tail on the left-hand side is suppressed by an upper cut on the Cherenkov angle. The deuteron peak is clearly visible.

2˙1. *The High Momentum Particle Identification Detector*. – The High Momentum Particle Identification Detector (HMPID) [18-20] performs charged hadrons (π, K, p) identification by means of the measurement of the emission angle of Cherenkov radiation and of the momentum information provided by the ALICE tracking devices. It is designed as a single-arm proximity-focusing Ring Imaging Cherenkov detector (RICH) where the radiator is a 15 mm thick layer of C_6F_{14} (perfluorohexane) with a refraction index of $n = 1.2989$ at the photon wave length $\lambda = 175\,\mathrm{nm}$ corresponding thus to the minimum particle velocity $\beta_{\mathrm{min}} = 0.77$. The HMPID, located at about 5 m from the beam axis, consists of seven identical counters covering in total an acceptance of about 5% at central rapidity.

Figure 2 (left) shows the Cherenkov angle from the HMPID as a function of the momentum in pp collisions at $\sqrt{s} = 7\,\mathrm{TeV}$. Figure 2 (right) shows an example of the Cherenkov angle distribution measured in the HMPID for positive tracks in a narrow p_T interval in pp collisions at $\sqrt{s} = 2.76\,\mathrm{TeV}$.
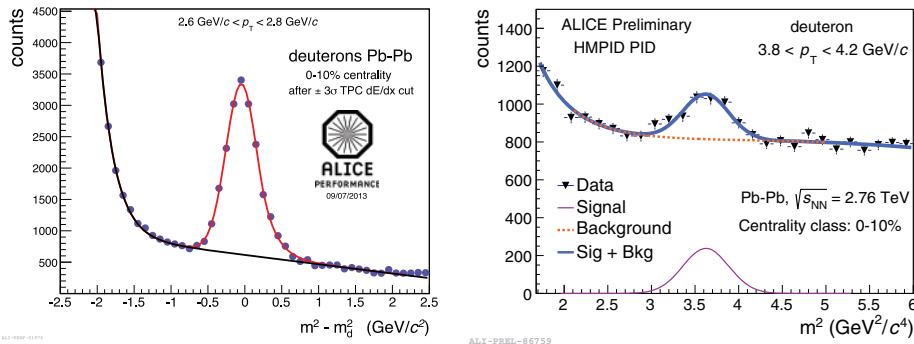
Fig. 4. – Left: distribution of $(m^2_{\mathrm{TOF}} - m^2_{\mathrm{d}})$ measured with the TOF detector (after a 3σ TPC dE/dx cut) for positive tracks with $2.6 < p_{\mathrm{T}} < 2.8\,\mathrm{GeV}/c$ in Pb-Pb collisions at $\sqrt{s_{\mathrm{NN}}} = 2.76\,\mathrm{TeV}$ (0–10% centrality class). The background from mismatched tracks (black solid line) is subtracted to obtain the raw yields. Right: distribution of m^2 measured with the HMPID detector for positive tracks with $3.8 < p_{\mathrm{T}} < 4.2\,\mathrm{GeV}/c$ in Pb-Pb collisions at $\sqrt{s_{\mathrm{NN}}} = 2.76\,\mathrm{TeV}$ (0–10% centrality class). The background (orange dotted line) is subtracted to obtain the raw yields. The peak corresponding to the deuteron mass is clearly visible for both distributions.

Figure 3 (right) shows the squared particle masses calculated from the momentum and Cherenkov angle reconstructed by the ITS-TPC and HMPID, respectively, for 10% most central Pb-Pb collisions at $\sqrt{s_{\mathrm{NN}}} = 2.76\,\mathrm{TeV}$ [21].

3. – Nuclei

Nuclei and anti-nuclei such as (anti-)deuterons, (anti-)tritons, and (anti-)^{3}He are identified using the specific energy loss measurement in the TPC as already shown in fig. 1 (see sect. **2**). The dashed curves represent a parametrization of the Bethe-Block function for the different particle species. The measured energy-loss signal of a track is required to be within 3σ from the expected value for a given mass hypothesis. This method provides a pure sample of ^{3}He nuclei in the relevant p_{T}-range between $2\,\mathrm{GeV}/c$ and $8\,\mathrm{GeV}/c$ and deuterons up to $1.4\,\mathrm{GeV}/c$.

Figure 4 (left) shows the $(m^2 - m^2_{\mathrm{d}})$ distribution for $2.6 < p_{\mathrm{T}} < 2.8\,\mathrm{GeV}/c$ obtained by matching of the TOF and TPC information. For each p_{T}-interval, this m^2-distribution is fitted with a Gaussian function with an exponential tail for the signal and an exponential function added to a first order polynomial for the background.

3`1. *Deuteron identification with HMPID detector*. – Deuterons and anti-deuterons are also identified at intermediate-p_{T}, namely in the range $3 < p_{\mathrm{T}} < 8\,\mathrm{GeV}/c$, in central Pb-Pb collisions by using the HMPID detector. The analysis in this case is limited by the available statistics and the (anti-)deuteron measurements are performed only in the 0–10% centrality class. The m^2-distributions are derived from the $\cos(\theta_{\mathrm{Cherenkov}}) = 1/(n\beta)$ and the momentum information from the tracking systems:

$$(1) \qquad\qquad m^2 = p^2(n^2 \cos^2 \theta_{\mathrm{Cherenkov}} - 1).$$

Figure 4 (right) shows the distribution of m^2-measured with the HMPID detector
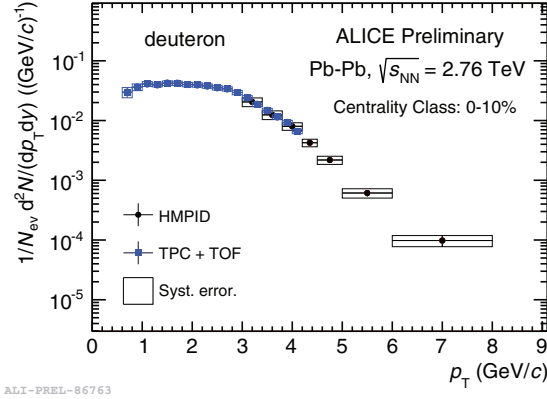
ALI-PREL-86763

Fig. 5. – Efficiency and acceptance corrected deuteron spectra using the TPC-TOF analysis (blue marker) and HMPID (black marker) in Pb-Pb collisions at $\sqrt{s_{NN}} = 2.76\,\text{TeV}$ in 0–10% centrality class. The agreement between the two different PID techniques, in the common p_T interval ($3 < p_T < 4.2\,\text{GeV}/c$), is within the uncertainties.

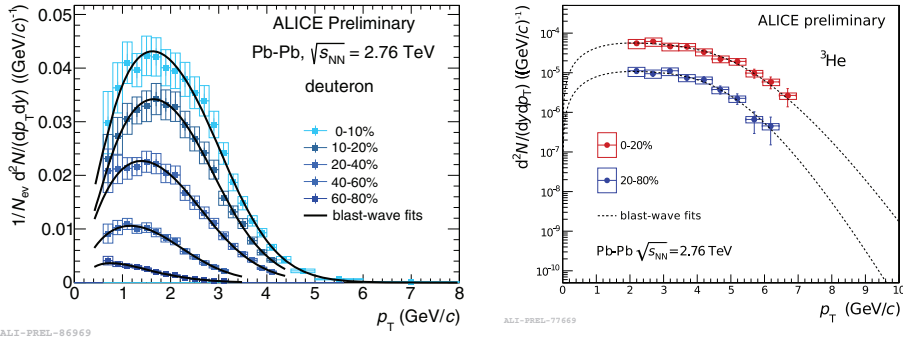ALI-PREL-86969   ALI-PREL-77669

Fig. 6. – Left: efficiency and acceptance corrected deuteron spectra for Pb-Pb collisions at $\sqrt{s_{NN}} = 2.76\,\text{TeV}$ in various centrality classes. The black lines represent an individual fit with the blast wave function. The boxes show the systematic error while the vertical lines represent the statistical error. Right: ^{3}He spectra for Pb-Pb collisions. The spectra are shown for two centrality classes (0–20% and 20–80%) and fitted individually with the blast wave function. The systematic and statistical uncertainties are shown by boxes and vertical lines, respectively.

for positive tracks with $3.8 < p_T < 4.2\,\text{GeV}/c$ in Pb-Pb collisions at $\sqrt{s_{NN}} = 2.76\,\text{TeV}$ (0–10% centrality class). In central Pb-Pb collisions, where the total number of hits in the HMPID is large, a Cherenkov ring could be reconstructed with hits incorrectly associated to the track, thus producing the significant background under the deuteron signal [18]. For each p_T-interval, the m^2-distribution is fitted with a Gaussian function for the signal and a negative power law function added to a third order polynomial for the background.

Figure 5 shows the comparison between the efficiency and acceptance corrected deuteron spectra measured with the TPC-TOF and HMPID for the 10% most central Pb-Pb collisions at $\sqrt{s_{NN}} = 2.76\text{TeV}$. The agreement between the two different PID techniques, in the common p_T interval ($3 < p_T < 4.2\,\text{GeV}/c$) is within the uncertainties.

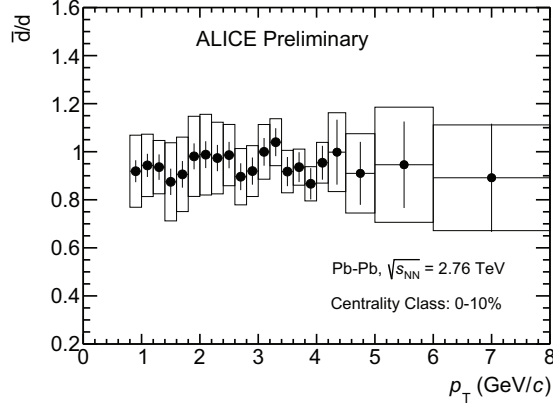Figure 6 shows efficiency and acceptance corrected spectra of d and ^{3}He, measured

Fig. 7. – Anti-deuteron–to–deuteron ratio as a function of transverse momentum in central Pb-Pb collisions. The boxes show the systematic error while the vertical lines represent the statistical error.
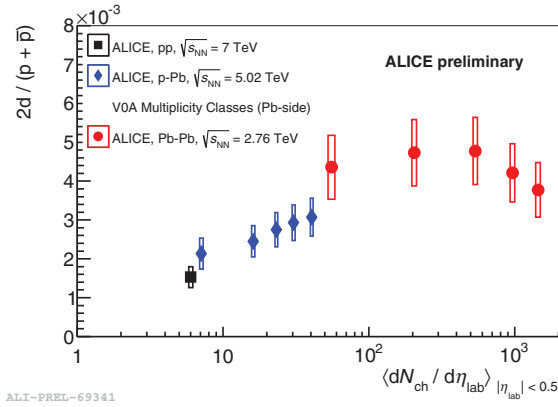

Fig. 8. – Deuteron-to-proton ratio as a function of charged-particle multiplicity at midrapidity.

in Pb-Pb collisions for different centrality selections. The p_T distributions show a clear evolution, becoming harder as the centrality increases, a behaviour similar to that of the protons which exhibit a significant radial flow [22]. The spectra obtained in Pb-Pb collisions are individually fitted with the blast wave model for the determination of p_T-integrated yields. Figure 7 shows the anti-deuteron to deuteron ratio as a function of the transverse momentum in central Pb-Pb collisions. The ratio exhibits a constant behavior as a function of p_T.

Figure 8 shows the deuteron-to-proton ratio as a function of the multiplicity in pp, p-Pb and in Pb-Pb collisions. The ratio rises with multiplicity until a possible saturation is reached for Pb-Pb collisions.

In the coalescence approach, light nuclei are formed after the kinetic freeze-out via coalescence of protons and neutrons which are near in space and with a low relative momentum. In this mechanism, the spectral distribution of the composite nuclei is
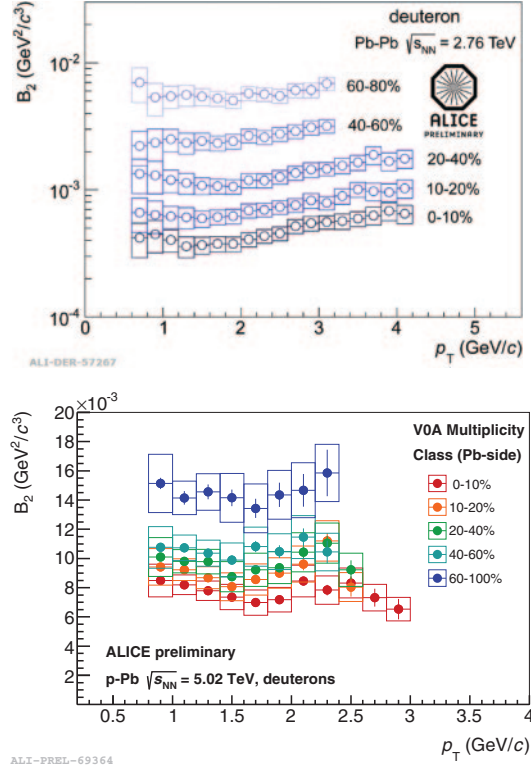
Fig. 9. – Coalescence parameter B_2 as a function of the transverse momentum per nucleon in Pb-Pb collisions at $\sqrt{s_{NN}} = 2.76$ TeV (top) and in p-Pb collisions at $\sqrt{s_{NN}} = 5.02$ TeV (bottom).

related to the one of the primordial nucleons via the following relationship:

$$(2) \qquad E_i \frac{\mathrm{d}^3 N_i}{(\mathrm{d}p_i)^3} = B_A \left(E_p \frac{\mathrm{d}^3 N_p}{(\mathrm{d}p_p)^3} \right)^A$$

assuming that protons and neutrons have the same momentum distribution. B_A is the coalescence parameter of particle i with mass number A and a momentum of $p_i = Ap_p$.

Figure 9 shows the obtained B_2 values for deuterons for Pb-Pb (the measurement is currently being extended to higher transverse momentum using the HMPID) and p-Pb (bottom) collisions. A clear decrease with increasing centrality is observed for Pb-Pb collisions. In the coalescence picture, this behaviour is explained by an increase in the source volume V_{eff}. B_2 also shows an increasing trend with the transverse momentum for central collisions, in contrast with the most simple coalescence models. This behaviour can be qualitatively understood by position-momentum correlations which are caused by a radially expanding source. In p-Pb collisions the B_2 is slightly decreasing with multiplicity, again in contrast with the most simple coalescence models.

REFERENCES

[1] CARMINATI A. *et al.* (ALICE COLLABORATION), *Physics Performance Report, Volume I*, *J. Phys. G: Nucl. Part. Phys.*, **30** (2004) 1517.
[2] ANDRONIC A., BRAUN-MUNZINGER P., STACHEL J. and STOECKER H., *Phys. Lett. B*, **697** (2011) 203.
[3] CLEYMANS J., KABANA S., KRAUS I., OESCHLER H., REDLICH K. *et al.*, *Phys. Rev. C*, **84** (2011) 054916.
[4] ANDRONIC A., BRAUN-MUNZINGER P., REDLICH K. and STACHEL J., *J. Phys. G*, **38** (2011) 124081.
[5] BUTLER S. and PEARSON C., *Phys. Rev.*, **129** (1963) 836.
[6] KAPUSTA J., *Phys. Rev. C*, **21** (1980) 1301.
[7] AFANASEV S. *et al.* (NA49 COLLABORATION), *Phys. Lett. B*, **22** (2000) 486.
[8] ADLER C. *et al.* (STAR COLLABORATION), *Phys. Rev. Lett.*, **87** (2001) 262301.
[9] SCHAEL S. *et al.* (ALEPH COLLABORATION), *Phys. Lett. B*, **639** (2006) 192.
[10] AKTAS A. *et al.* (H1 COLLABORATION), *Eur. Phys. J. C*, **36** (2004) 413.
[11] ABRAMOV V., BALDIN B. Y., BUZULUTSKOV A., GLEBOV V. Y., DYSHKANT A. *et al.*, *Sov. J. Nucl. Phys.*, **45** (1987) 845.
[12] ANTICIC T. *et al.* (NA49 COLLABORATION), *Phys. Rev. C*, **69** (2004) 024902.
[13] BEARDEN I. G. *et al.*, *Phys. Rev. Lett.*, **85** (2000) 2681.
[14] SCHEIBL R. and HEINZ U. W., *Phys. Rev. C*, **59** (1999) 1585.
[15] STEINHEIMER J., GUDIMA K., BOTVINA A., MISHUSTIN I., BLEICHER M. and STOCKER H., *Phys. Lett. B*, **85** (2012) 714.
[16] ALESSANDRO B. *et al.* (ALICE COLLABORATION), *Physics Performance Report, Volume II J. Phys. G. Nucl. Part. Phys.*, **32** (2006) 1295.
[17] AAMODT K. *et al.* (ALICE COLLABORATION), *J. Instrum.*, **3** (2008) SO8002.
[18] ABELEV B. *et al.* (ALICE COLLABORATION), *Phys. Lett. B*, **736** (2014) 196.
[19] BARILE F. for the ALICE COLLABORATION, *Proceedings of the 13th ICATPP Conference* (World Scientific Publishing Co. Pte. Ltd.) 2012 pp. 445-449.
[20] BARILE F., CERN-THESIS-2012-263, PhD Thesis (2012).
[21] ABELEV B. *et al.* (ALICE COLLABORATION), *Int. J. Mod. Phys. A*, **29** (2014) 1430044.
[22] ABELEV B. *et al.* (ALICE COLLABORATION), *Phys. Rev. Lett.*, **111** (2013) 222301.